Metadata of the chapter that will be visualized online

Series Title		
Chapter Title	Evolution of the Cell's Mechanical Design	
Chapter SubTitle		
Copyright Year	2011	
Copyright Holder	Springer Science + Business Media B.V.	
Corresponding Author	Family Name	Boal
	Particle	
	Given Name	**David**
	Suffix	
	Division	Department of Physics
	Organization	Simon Fraser University
	Address	V5A 1S6, Burnaby, BC, Canada
	Email	
Author	Family Name	Forde
	Particle	
	Given Name	**Cameron**
	Suffix	
	Division	Department of Physics
	Organization	Simon Fraser University
	Address	V5A 1S6, Burnaby, BC, Canada
	Email	

Abstract	The mechanical properties of the cell's structural components influence the size, shape, and functionality of the cell throughout its division cycle. For example, a combination of the plasma membrane's edge tension and bending resistance sets a lower bound on cell size, while the membrane's tear resistance sets a pressure-dependent upper bound on the size of cells lacking a cell wall. The division cycle of the simplest cells may be dominated by one or two principles such as the maximization of entropy, or the minimization of energy or structural materials. By studying colonies of cells, modern and fossilized, with techniques from classical and statistical mechanics, a partial history can be charted for the appearance and properties of the simplest cell designs.

Keywords (separated by '-')	Cell mechanics - membrane elasticity - microfossils - cell division cycle

Chapter 2
Evolution of the Cell's Mechanical Design

David Boal and Cameron Forde

Abstract The mechanical properties of the cell's structural components influence the size, shape, and functionality of the cell throughout its division cycle. For example, a combination of the plasma membrane's edge tension and bending resistance sets a lower bound on cell size, while the membrane's tear resistance sets a pressure-dependent upper bound on the size of cells lacking a cell wall. The division cycle of the simplest cells may be dominated by one or two principles such as the maximization of entropy, or the minimization of energy or structural materials. By studying colonies of cells, modern and fossilized, with techniques from classical and statistical mechanics, a partial history can be charted for the appearance and properties of the simplest cell designs.

Keywords Cell mechanics • membrane elasticity • microfossils • cell division cycle

2.1 Introduction

The sizes and shapes of cells have become more diverse with the passage of geological time, built around a core of micron length scales and morphologies such as rods, diplococci and filaments that appeared early in the Earth's history. Yet the incredibly slow change in cell dimensions is suggestive of optimization – that certain structural designs are most appropriate for the complete chemical and physical environment in which cells grow. The factors that must influence the design include ease of construction and repair, appropriate strength and permeability, availability of a mechanically feasible division cycle etc. Further, there may be physical principles at play, such as energy minimization or materials minimization, and the relative importance of each principle may depend on cell morphology or design.

D. Boal (✉) and C. Forde
Department of Physics, Simon Fraser University, V5A 1S6 Burnaby, BC, Canada

P.L. Luisi and P. Stano (eds.), *The Minimal Cell: The Biophysics of Cell Compartment and the Origin of Cell Functionality*, DOI 10.1007/978-90-481-9944-0_2,

The maximization of entropy provides a simple example of how a physical principle can drive the division cycle. If the area of the cell's boundary (its membrane and cell wall, if present) grows as fast as its volume, then at some point the surface will form entropy-producing arms and channels, as shown in the computer simulation of Fig. 2.1, a category of shapes known as branched polymers. If the arms are physically able pinch off to form individual cells, then the entropy-driven formation of branched polymer shapes can be the basis of a very simple cell division cycle. Of course, this design is not at all efficient in the usage of materials: there is a metabolic cost to producing cell boundary material and the boundary area of branched polymer shapes is rather large before cell division is achievable. Among other cell shapes, diplococci, rods, filaments have division cycles that are more materials efficient than branched polymers.

In this chapter, we examine the mechanical properties of the structurally simplest cells. In Section 2.1, the most important structural components are identified and their properties as a function of cell size are analyzed using results from continuum mechanics. For example, we describe the surface stress experienced by a cell under elevated interior pressure and examine the deformation energy of a lipid bilayer. Section 2.2 addresses the question of how the construction of cells has changed in the past three billion years (3 Ga). In this section, we analyze the bending resistance of 2–3 Ga biofilaments using a technique originating in statistical mechanics, and we demonstrate the consistency of design in both ancient and modern filamentous cyanobacteria, as well as estimate some bounds on the mechanical properties of these filamentous cells. In Section 2.3 we examine a number of models for the cell division cycle that focus on the changes in cell shape during growth and division. We show how to extract the time evolution of a system by measuring the instantaneous properties of an ensemble of cells with steady-state growth. This methodology is then applied in Section 2.4 to diplococci in order to study the division cycles of 2 Ga microfossils and modern cyanobacteria. Our conclusions are summarized in Section 2.5.

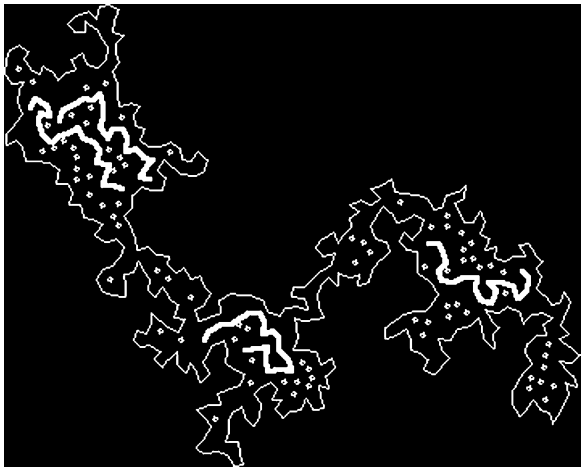

Fig. 2.1 Computer simulation of entropy-driven cell division in two dimensions. Enclosed within this cell are four genetic polymers (*linked spheres*) as well as numerous solvent spheres. Entropy-laden arms only appear when the perimeter of the cell becomes large (Boal and Jun unpublished)

2.2 Mechanical Features of a Simple Cell

Consider as a model system a very simple cell design in which there are only one or two structural components: (1) a fluid membrane that bounds the cell and isolates its components from the environment, and perhaps (2) a shear-resistant wall attached to the fluid membrane. By the word "fluid" we mean a two-dimensional structure that has no shear resistance in its plane: for example, the chocolate coating on a cherry freshly dipped in liquid chocolate is effectively a two-dimensional fluid in that the chocolate can flow to adapt to the shape of the cherry. In contrast, a child's balloon resists shear in the plane of the rubber membrane, even though that membrane can be highly deformed by the pressure of the balloon. The interior of this simple cell may be under elevated osmotic pressure, just like modern bacteria, and the larger the cell is, the more likely the fluid membrane must be augmented by a structure like a cell wall with high tensile strength. We now examine several mechanical properties of fluid membranes.

2.2.1 Bending Resistance of a Membrane

The lipid bilayer that forms the (two-dimensional) fluid boundary of the cell is a self-assembled structure whose equilibrium configuration is spatially flat if the molecular composition is the same within both leaflets of the bilayer. Efforts to bend an initially flat bilayer require the outlay of an energy cost per unit area E whose simplest parametrization is (Helfrich 1973)

$$\mathrm{E} = (k/2)(1/R_1 + 1/R_2)^2 + k_{\mathbf{G}}/R_1R_2, \qquad (2.1)$$

where the constants κ (bending rigidity) and κ_G (Gaussian curvature modulus) have units of energy. The quantities R_1 and R_2 are the two principal radii of curvature; for example, a sphere of radius R has $R_1 = R_2 = R$, while a cylinder of radius R has $R_1 = R$ around the circumference and $R_2 = \infty$ (i.e. no curvature) along the axis of symmetry. To find the bending energy of a particular surface, one simply integrates E over the area of the surface; hence the deformation energy of a spherical shell of radius R is $8\pi\kappa + 4\pi\kappa_G$, independent of R. Lipid bilayers in conventional cells are found to have $\kappa = 10$–$25\ k_BT$, where k_B is Boltzmann's constant and T is the absolute temperature (Evans and Rawicz 1990). The value of κ_G is less well known, but expected to have a similar value to κ. Thus, the deformation energy of a bilayer formed into a spherical shell is $12\pi\kappa = 250$–$600\ k_BT$ when $\kappa = \kappa_G$. Although this is not a huge amount of deformation energy, why would lipid bilayers spontaneously deform at all to form a simple cell? To answer this question, we next look at the so-called edge tension of a bilayer.

2.2.2 Edge Tension of a Bilayer

A fluid membrane not only resists bending, it also resists stretching and will rupture once its area has been stretched by more than a few percent from its unstressed value.

The creation of a hole in a membrane likely involves reconfiguring the lipid molecules around the boundary of the hole in order to reduce contact between the aqueous medium surrounding the bilayer and the water-avoiding hydrocarbon chains of the lipid molecules that are normally hidden within the bilayer. In general, the orientation of the lipids at the hole boundary is energetically unfavorable compared to their orientation in an intact bilayer: that is, there is an energy penalty for creating a hole. The boundary of the hole can be characterized by an edge tension λ (energy per unit length along the boundary), such that the energy of the hole is equal to λ times its perimeter. Measured values of λ are in the 10^{-11} J/m range; which is larger than the minimum λ required for membrane stability as estimated from computer simulations of membrane rupture (Boal and Rao 1992).

2.2.3 *Minimal Cell Size to Close a Bilayer into a Sphere*

The energy of the membrane boundary and the energy of membrane bending have a different dependence on the physical size of the membrane, with the result that a flat membrane must reach a minimum size before it becomes energetically favorable for the membrane to close up into a sphere. In detail, consider a membrane in the shape of a flat disk of radius R_{disk}, perimeter $2\pi R_{\text{disk}}$, and consequently, total edge energy $2\pi R_{\text{disk}}\lambda$. This shape will be energetically favored over a closed sphere with bending energy $12\pi\kappa$ (when $\kappa = \kappa_G$) so long as $R_{\text{disk}} < 6\kappa/\lambda$. Since we are more interested in the dimensions of closed spheres than flat disks, we replace R_{disk} by $2R_{\text{sphere}}$ which applies when the disk and sphere have the same area. Thus, the minimum radius of a closed sphere within this description of membrane energetics is $R_{\text{sphere}} > 3\kappa/\lambda$ (after Fromhertz 1983). Typical values of $\kappa \sim 15\ k_B T$ and $\lambda \sim 10^{11}$ J/m lead to the condition $R_{\text{sphere}} > 20$ nm, which is somewhat less than the minimal size found for pure bilayer vesicles obtained in laboratory studies. Once the membrane has adopted the shape of a sphere, the configuration could be further stabilized by the addition of lipids to the outer leaflet of the bilayer, thus reducing the strain created by the bending deformation.

2.2.4 *Maximal Size for Wall-Less Cells Under Pressure*

In a child's balloon or a bicycle tire, the pressure from the confined gas creates a stress within the rubber membrane that forms the boundary of the system. The rubber membrane can be regarded as an effectively two-dimensional system because its thickness is much smaller than its lateral dimensions. Within the plane of the membrane, then, there is a (two-dimensional) surface stress Π having units of energy per unit area. For a spherical shell supporting a pressure difference P across the shell, the surface stress is given by

$$\prod = PR/2, \tag{2.2}$$

where R is the radius of the sphere and P has units of energy per unit volume, as usual for a three-dimensional stress. Equation (2.2) tells us that for a fixed pressure difference, the smaller the radius of the sphere, the smaller the surface stress. This is the reason why a simple bacterium can support an osmotic pressure of several atmospheres without needing a cell wall as thick as a tire.

When subjected to a surface stress, a membrane first stretches and then ruptures: depending on their composition, lipid bilayers typically rupture at Π around 1×10^{-2} J/m^2 on laboratory time scales (Needham and Hochmuth 1989). For a spherical cell of radius $R = 1$ μm and no cell wall, rupture occurs at a fairly low osmotic pressure: Equation (2.2) predicts that the pressure at a failure stress of $\Pi = 10^{-2}$ J/m^2 would be 2×10^4 J/m^3 = 0.2 atm. Thus, a bacterium requires a cell wall to support an osmotic pressure of several atmospheres, which is more than the lipid bilayer of the plasma membrane can withstand. However, such is not the case for smaller cells: the same type of calculation shows that a pure bilayer vesicle of just 100 nm (or diameter 0.2 μm) could operate at an osmotic pressure of 2 atm. without needing a cell wall for additional strength (Boal 2002).

2.2.5 *Bending and Packaging of DNA*

Modern cells carry their genetic blueprint as DNA, which has a contour length that well exceeds the linear dimension of the cell itself. As a double-stranded helix, DNA is considerably stiffer than a simple flexible polymer like a saturated alkane, such that for eukaryotic cells such as our own, the packaging of DNA inside the cell is a challenge. The stiffness of a linear filament is often characterized through its bending rigidity κ_f or its persistence length ξ; we use the latter representation in this section and introduce κ_f in Section 2.2. Mathematically, the persistence length is a measure of the length scale over which the orientation of a curve undergoes a significant change in direction. For molecules whose variation in shape is governed by thermal fluctuations, ξ and κ_f are directly proportional to each other through $\xi = \kappa_f / k_B T$, from which one sees that the stiffer the filament (larger κ_f) the longer the persistence length.

If a filament with a specific value of ξ undergoes random changes in direction all along its contour length L_c, then the root mean square value of the displacement $\mathbf{r}_{ee}$ between the positions of the two ends of the filament is given by

$$< r_{ee}^2 >= 2\xi L_c, \tag{2.3}$$

where the notation $< ... >$ implies than an ensemble average has been made from a selection of all observed configurations. Equation (2.3) tells us that the stiffer the filament (larger ξ) the greater the end-to-end displacement for a fixed contour length. Let's apply this to the DNA of *E. coli*, whose DNA contains 4.7 million base pairs; at 0.34 nm per base pair, this strand of DNA has a contour length of 1.6×10^6 nm. The persistence length of DNA is quoted as about 53 nm (Bustamante et al. 1994), so Eq. (2.3) predicts that the root mean square end-to-end displacement of an open strand of DNA of *E. coli* is givven by $< r_{ee}^2 >^{1/2} = 13 \mu$m, not that much larger than the physical size of the bacterium itself.

A related measure of the size of a flexible filament is its radius of gyration, R_g, which is defined by $< R_g^2 >= N^{-1} \sum_{i=1,N} r_i^2$, where the filament has been appropriately sampled at N points with displacements $\mathbf{r}_i$ from the center-of-mass position of the filament. If the physical overlap of remote sections of the filament is permitted, then randomly oriented filaments are governed by $< R_g^2 >=< r_{ee}^2 > /6 = \xi L_c / 3$. For example, we would expect $< R_g^2 >^{1/2} = 5.3 \mu$m for the DNA of *E. coli* given the value for $< r_{ee}^2 >$ calculated in the *E. coli* example above. A similar calculation for mycoplasma, a very small cell with 800,000 base pairs of DNA, yields $< R_g^2 >^{1/2} = 2.2 \mu$m. For both of these structurally simple cells, the effective size of a ball of their DNA is roughly the same linear dimension as the cell itself. However, this is not the case for eukaryotic cells: human DNA is much longer than bacterial such that it takes up far more volume in the cell as a random coil. Consequently, advanced cells have developed a packaging technique in which their DNA is wrapped around barrel-shaped proteins called histones, with a diameter of 11 nm, in order to organize and sequester their long genetic blueprints.

The examples in this section (the constraints on cell size, the need for cell walls to maintain cell integrity, the packaging of DNA) all illustrate the influence of cell mechanics and construction on the stability and function of the cell.

2.3 Structural Evolution of Filamentous Cells

We now turn our attention to how the design and construction of cells has changed over time, using as our guide a comparison between modern cyanobacteria and microfossils more than two billion years old. The approach is not so much to make statistical comparisons between cell shapes, but rather to determine, where feasible, mechanical characteristics of cells before they were fossilized and chart the evolution of these characteristics. In this section, we focus on the elastic properties of filamentous cells; in Section 2.4 we investigate the cell cycles of diplococci and rod-like cells.

First appearing more than three billion years ago, filament-forming cells have been present throughout much of the Earth's history (Cloud 1965; Barghoorn and Schopf 1966; Walsh and Lowe 1985; Schopf and Packer 1987; Schopf 1993; Rasmussen 2000). Three examples of two-billion-year-old filamentous structures are displayed in Fig. 2.2: parts (a) and (b) are *Gunflintia minuta* Barghoorn and *Gunflintia grandis* Barghoorn, respectively (Barghoorn and Tyler 1965; author's specimens from Lake Superior, Canada) and part (c) is *Halythrix* Schopf (Schopf 1968; specimen from Belcher Islands, Canada, in Hofmann 1976). Even older examples of filamentous structures include 3.23 Ga pyritic replacement filaments (Rasmussen 2000). The original internal construction of these filaments has been destroyed or modified by the fossilization process, but that doesn't mean that their native mechanical properties cannot be probed by other means. Based solely on the analysis of static images, several techniques are available for determining the mechanical behavior of cells, and these approaches are equally adaptable to microfossils as they are to living cells.

The technique that we examine most closely in this section is the tangent correlation length ξ_t that can be related to the resistance of a filament against

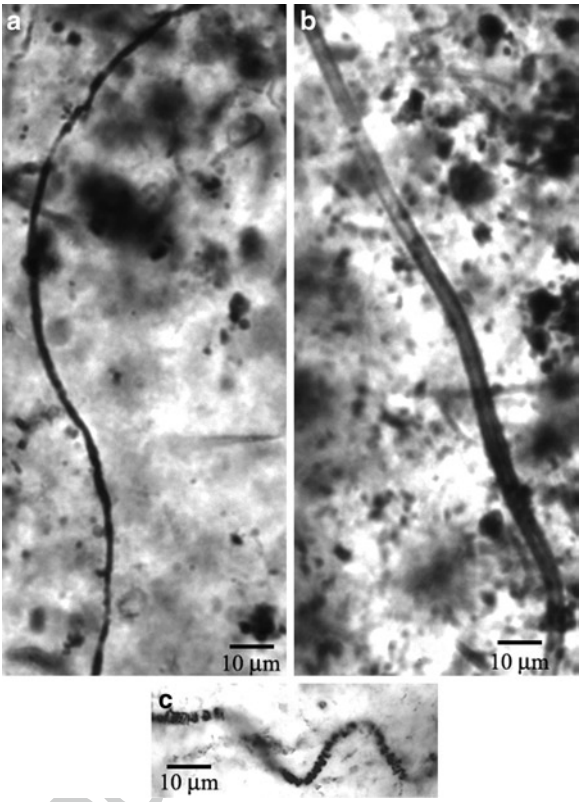

Fig. 2.2 Examples of *Gunflintia minuta* (**a**) and *Gunflintia grandis* (**b**) from GSC 10913c (Schreiber, Ontario, Canada; Boal and Ng unpublished); *Halythrix* (**c**) from GSC 42769 (Belcher Islands, Canada; reported by Hofmann 1976). Scale bar is 10 µm in all images

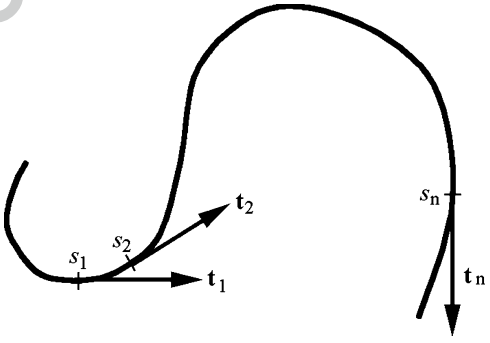

Fig. 2.3 Unit tangent vectors ($\mathbf{t}_1$, $\mathbf{t}_2$, $\mathbf{t}_n$) at arc lengths (s_1, s_2, s_n) along a sinuous curve. Separations between the locations $\Delta s = |s_2 - s_1|$ are distances, not displacements

bending. To see how this works, consider the changes in the local orientation of the sinuous curve illustrated in Fig. 2.3 as recorded through the behavior of the tangent vector $\mathbf{t}(s)$ at location s along the curve, where $\mathbf{t}$ has unit length according to the dot product $\mathbf{t} \bullet \mathbf{t} = 1$. If two location s_1 and s_2 are close to each other on the curve, then $\mathbf{t}(s_1)$ and $\mathbf{t}(s_2)$ have similar directions and their dot product is close to unity. On the other hand, if s_1 and s_2 are far apart along the curve (even though they may be close spatially) their tangent vectors may point in quite different directions and $\mathbf{t}(s_1) \bullet \mathbf{t}(s_2)$

may vary between −1 and +1. The average behavior of $\mathbf{t}(s_1) \bullet \mathbf{t}(s_2)$ is contained in the tangent correlation function $C_t(\Delta s)$,

$$C_t(\Delta s) \equiv < t(s_1) \bullet t(s_2) > . \tag{2.4}$$

The ensemble average indicated by the brackets $< \ldots >$ on the right hand side of this equation is performed over all pairs of points s_1 and s_2 subject to the constraint that $|s_2 - s_1|$ is equal to a particular Δs specified on the left hand side. When s_1 and s_2 are nearby ($\Delta s \cong 0$), the ensemble average over $\mathbf{t}(s_1) \bullet \mathbf{t}(s_2)$ is necessarily close to unity, whereas when Δs is so large such that the tangent orientations are random with respect to each other, the average is close to zero. For a variety of very general situations, this behavior of $C_t(\Delta s)$ at small and large Δs is described by exponential decay in Δs (see Doi and Edwards 1986 or Boal 2002):

$$C_t(\Delta s) = \exp(-\Delta s / \xi_t). \tag{2.5}$$

The length scale for the correlations is provided by the tangent correlation length ξ_t: the more sinuous the curve, the smaller is ξ_t. For filaments whose shapes are governed by thermal fluctuations in their deformation energy, the correlation length ξ_t of Eq. (2.5) is the same as the persistence length of Eq. (2.3). As a technical aside, it should be mentioned that correlation function depends on the dimensionality of the system: the true correlation length ξ_3 of a filament in three dimensional space is related to the correlation length ξ_{2p} of the same filament whose shape is projected into two dimensions via $\xi_3 = (3\pi/8)\, \xi_{2p}$.

Now, the magnitude of the deformation of a filament in response to a shear stress is inversely proportional to the filament's stiffness or, properly speaking, its *flexural rigidity* κ_f: the stiffer the filament, the smaller the deformation. To be specific, the deformation energy per unit length for bending a uniform rod is equal to $\kappa_f/2$ multiplied by the square of the rate of change of the tangent direction along the filament contour. It can be established that the flexural rigidity of a uniform solid cylinder of radius R is given by (see Boal 2002)

$$k_f = \pi Y R^4 / 4, \quad \text{(solid cylinder)} \tag{2.6}$$

where Y is the Young's modulus of the material; typically $Y \sim (1\text{–}5) \times 10^8$ J/m^3 for soft biomaterials. For a hollow cylinder of outer radius R bounded by a wall of thickness t, the flexural rigidity can be approximated by

$$k_f = \pi Y R^3 t, \quad \text{(hollow cylinder)} \tag{2.7}$$

when $t << R$. Thus, the flexural rigidity grows as R^3 or R^4 for these two simple shapes. Given that the energetic cost of the deformation is proportional to κ_f, it would not be surprising if the tangent correlation length ξ_t is also proportional to R^3 or R^4, as a benchmark.

Two correlation functions obtained from microfossils are shown in Fig. 2.4 for projected filament trajectories in two dimensions, leading to the determination of the correlation length ξ_{2p}; the figure shows both the raw data as well as their fit with an

[AU1] exponential function (Boal and Ng unpublished). Two taxa from the Gunflint Formation are displayed in the figure: *G. minuta*, the narrower of the two, is found to have $\xi_{2p} = 670 \pm 40$ μm, while the wider *G. grandis* has a shorter ξ_{2p} of 330 ± 30 μm for a particular subset of the *G. grandis* filaments (there may be two populations of filaments in the group that are now collectively assigned as *G. grandis*, the *S* subset has a smaller mean diameter than the genus as a whole, while the *L* subset has a larger mean diameter). In both cases, ξ_{2p} is a remarkable two orders of magnitude larger than the diameter of the filament itself, a ratio of ξ_t:*R* that is common among both microfossils and modern cells. For comparison, Fig. 2.5 shows the tangent correlation lengths of three genera of modern cyanobacterial filaments that represent three very different cell geometries (*Geitlerinema*, *Pseudanabaena*, and *Oscillatoria*, from smallest to largest filament diameter). Both *Geitlerinema* and *Oscillatoria* exhibit values of ξ_2 that rise with filament diameter among species of the genus.

Equations (2.6) and (2.7) demonstrate that κ_t depends most strongly on the filament radius, as R^3 or R^4 for the two idealized systems that we have considered.

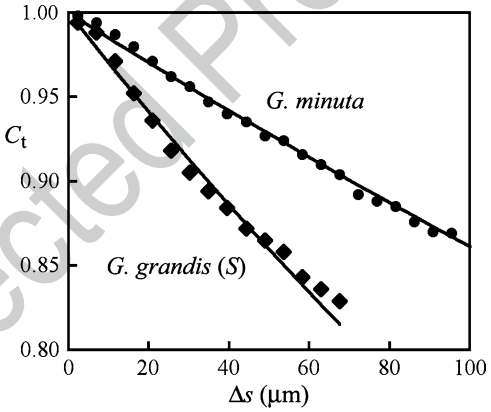

Fig. 2.4 Tangent correlation function $C_t(\Delta s)$ as a function of separation Δs (in micrometer) obtained by weighted average for *G. minuta* (*disks*) and the *S* group of *G. grandis* (*diamonds*). The solid curves are the exponential decays predicted by Eq. (2.5) with $\xi_{2p} = 670$ and 330 μm for *G. minuta* and the *S* group of *G. grandis*, respectively (Boal and Ng unpublished)

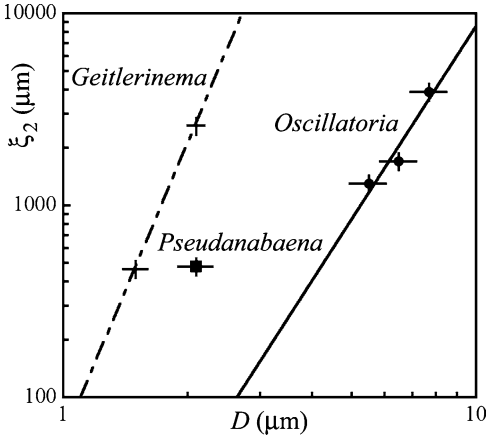

Fig. 2.5 Measured ξ_2 (in micrometer) for filamentous cyanobacteria as a function of their mean diameter *D*. The correlation functions are approximately described by $4.3 \bullet D^{3.3 \pm 1}$ for *Oscillatoria* and $62 \bullet D^{5.1 \pm 1}$ for *Geitlerinema* (*solid and dot-dashed lines*, respectively; both *D* and the result are in micrometer). The cyanobacteria are *Geitlerinema* (*crosses*), *Pseudanabaena* (*square*), and *Oscillatoria* (*disks*) (Boal and Ng unpublished)

There are structural differences among even the three genera in Fig. 2.5, so the most likely behavior of κ_f is that the species within a given genus obey a particular R^n scaling, but the proportionality constant will vary from one genus to another. For a filament subject only to thermal fluctuations in its deformation energy, the correlation length ξ_t is linearly proportional to the flexural rigidity κ_f. We assume that this proportionality is also valid here, so that the anticipated functional form of the correlation length is $\xi_t = CR^n$ (where the proportionality constant C varies with the genus). Hence, a log-log plot of ξ_t versus R should be a straight line with a slope of 3 or 4 associated with the power-law dependence of κ_f on R.

The two straight lines shown in Fig. 2.5 are the functions

$$\xi_2 = 62 \bullet D^{5.1\pm1} \quad (\textit{Geitlerinema}) \tag{2.8}$$

$$\xi_2 = 4.3 \bullet D^{3.3\pm1}, \quad (\textit{Oscillatoria}) \tag{2.9}$$

where D is the filament diameter quoted in microns, and the result for ξ_2 is also in microns (Boal and Ng unpublished). The exponents in these functional forms, 5.1 ± 1 and 3.3 ± 1, are seen to be in good agreement with the expectations from continuum mechanics for the R-dependence of the flexural rigidity. Yet Eqs. (2.8) and (2.9) are obviously not identical, indicating that there is a genus-dependence to the behavior of the correlation length ξ_2. One characteristic that distinguishes among the three genera of Fig. 2.5 and that might contribute to the difference between Eqs. (2.8) and (2.9) is the mean length-to-width ratio of the individual cells: roughly four for *Geitlerinema*, 1.5–2 for *Pseudanabaena* and 0.7 for *Oscillatoria*. Thus, at a given filament diameter, ξ_2 increases with the length-to-width ratio of the cell in Fig. 2.5. Given the very large difference between the cell length-to-width ratios of *Geitlerinema* and *Oscillatoria*, it may be that these two genera lie near two distinct soft limits for the range of tangent correlation lengths available to cellular filaments. That is, with its large length-to-width ratio of individual cells, *Geitlerinema* may represent one limit, while the small length-to-width ratio of *Oscillatoria* represents the opposite limit.

Let's now compare the behavior of modern filamentous cyanobacteria in Fig. 2.5 with the measured correlation lengths of microfossils as displayed in Fig. 2.6. The first observation is that the tangent correlation lengths of the microfossil taxa *Gunflintia* and *Eomycetopsis* are easily in the same range as modern filamentous cyanobacteria. At 700 ± 100 μm, ξ_{2p} of *E. filiformis* is not far from Eq. (2.8) for ξ_2 of *Geitlerinema* represented by the dot-dashed line on the figure. These two types of filaments also have a similar visual appearance as tube-like structures. In addition, *E. filiformis* is not that far removed from $\xi_2 = 480 \pm 50$ of modern *Pseudanabaena* PCC 7403, although *Pseudanabaena* possesses marked indentations at the cell division planes while *E. filiformis* does not. The three variants of *Gunflintia* in Fig. 2.6 have correlation lengths in the 300–700 μm range for populations with apparent diameters of 1–4 μm: *G. minuta* lies near Eq. (2.8) for *Geitlerinema* while the *L* subgroup of *G. grandis* lies near Eq. (2.9) for *Oscillatoria*. All of the *Gunflintia* microfossils lie within the soft boundaries provided by Eqs. (2.8) and (2.9) for the most likely domain of correlation lengths. At less than 50 μm, the very short tangent

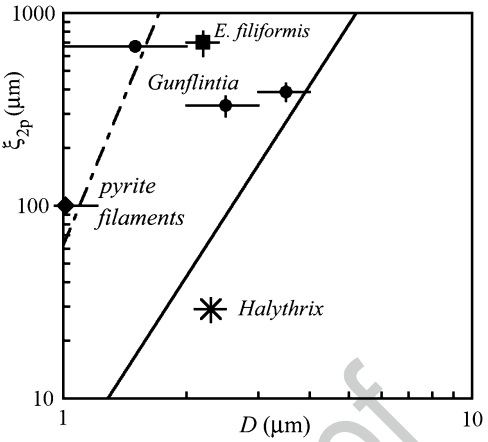

Fig. 2.6 Measured ξ_{2p} (in micrometer) for microfossil filaments as a function of their mean diameter. The curves $4.3 \bullet D^{3.3 \pm 1}$ and $62 \bullet D^{5.1 \pm 1}$ (both D and the result are in micrometer) are drawn for reference and also appear in Fig. 2.10. The filaments are *Gunflintia* (*disks*), *Halythrix* (*cross*), and *E. filiformis* (*square*); pyritic replacement filaments are indicated by the diamond near the *y*-axis (Boal and Ng unpublished)

correlation length of the taxon *Halythrix* is much lower than the range found among the selection of modern cyanobacteria in Fig. 2.6, although it is not that far removed from the extrapolated fit to *Oscillatoria* in the figure.

The figure also displays ξ_{2p} from 3.23 Ga pyritic replacement filaments observed in a volcanogenic massive sulphide deposit (Rasmussen 2000). The magnitude of ξ_{2p} determined for these objects is below *Gunflintia* and *E. filiformis* by factors of three or more, although it is still larger than *Halythrix*. However, pyritic replacement filaments are also relatively narrow, and the combination of their width and tangent correlation length is completely consistent with an extrapolation of the empirical description of ξ_2 of *Geitlerinema*, as can be seen from Fig. 2.6, although this is not proof that the pyritic filaments had a biological origin.

The analysis of filament shapes demonstrates the similarity of the rigidity of both modern filamentous cyanobacteria and filamentous microfossils reaching back billions of years: most of the filaments exhibit a tangent correlation length that is one or two orders of magnitude greater than their radius. However, the similarity of their tangent correlation lengths by itself does not imply that these microfossil taxa must be cyanobacteria, as the correlation lengths of eukaryotic green algae with similar diameters also lie in this range; for example, $\xi_2 = 900 \pm 100$ nm for the green alga *Stichococcus* with a mean diameter of 3.5 ± 0.2 μm (Boal and Forde [AU2] unpublished). What this analysis does demonstrate is that the some aspects of the design of filamentous cells probably emerged fairly early in the history of life, and that filaments represent a robust and adaptable cell design.

2.4 Models for the Cell Division Cycle

At the molecular level, the materials suitable for the construction of cells must satisfy constraints imposed by the need for at least some of the cell's structural components to self-assemble and the need for the cell to change shape during the division cycle. At its simplest level, the division cycle only requires that the mean

volume V and area A of the cell double independently during the cycle once a steady-state growth pattern has been achieved. These changes in the area and volume of the cell can be accommodated through the use of a (two-dimensional) fluid boundary such as a lipid monolayer or bilayer, which has the flexibility to change shape as needed with a minimal cost in deformation energy. An illustration of a division cycle that even a fluid *mono*layer can support is displayed in Fig. 2.1: the monolayer grows by the random addition of new molecules and ultimately forms wavy arms that can pinch off to form new cells, assuming that the cell's genetic blueprint has been replicated on the same time scale as the growth in cell size. The main physical principle that drives this model cycle is one that nature adores: the maximization of entropy (simulation by Boal and Jun unpublished; see Luisi 2006 [AU3] and Zhu and Szostak 2009 for overviews of related experimental work).

The cell shape displayed in Fig. 2.1 belongs to a family of random shapes that obey branched polymer scaling, where the surface area is proportional to the enclosed volume, unlike a spherical balloon where $A \sim V^{2/3}$. However, these shapes are not efficient in the usage of materials: it isn't so much that the surface area grows so fast, but rather that the cell must be sufficiently large before (i) the branched polymer shapes emerge, and (ii) its genetic blueprints have replicated and separated. Given that cells must expend metabolic energy to produce the molecules composing the cell boundary, other routes to cell division may be more appropriate. One possible design is based on the use of molecules that, perhaps because of their spatial conformation, generate a membrane that is naturally deformed. For instance, a sphere of radius R has a surface with curvature $C = 1/R$. Suppose a membrane is made from molecules that favor surfaces that spontaneously deform to some particular curvature C_o. As more molecules are added to this membrane, it grows at constant curvature in the form of two overlapping spherical caps linked together at a ring with radius less than $1/C_o$, until the ring closes, leaving just two touching spheres. Now, this design is not flawless, in that the membrane curvature in the intersection region of the ring has the wrong sign – if the surface is concave (inwardly curved) over most of the linked spheres, it is convex (outwards) along the intersection ring itself, like the shape of an old-fashioned hour-glass.

Another group of materials-efficient cell designs is based on systems with two mechanical components. These components need not possess distinct molecular composition, but rather need to move independently of one another over some range of shapes. Even a bilayer composed of only one type of lipid is sufficient, so long as the time scale for lipid molecules to migrate between leaflets of the bilayer is sufficiently long. Consider, for example, the bilayer structures with symmetric molecular composition shown in Fig. 2.7. If the inter-leaflet migration of molecules is slow, then material produced within the cell can be added to the inner leaflet without immediately transferring to the outer one. For a short time, the inner leaflet can accommodate more molecules without increasing its area, resulting in an increase in its molecular density and, correspondingly, its state of strain. However, this strain can be relieved through buckling, which adds a ring of material to the inner leaflet, as shown in cross-section in Fig. 2.7b. Although there is deformation energy associated with the region where the ring joins the spherical shape of the inner leaflet,

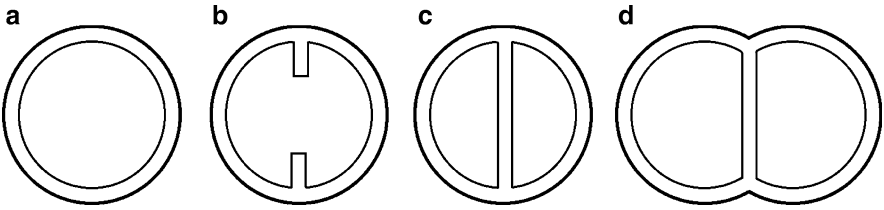

Fig. 2.7 One possible model for the division cycle of a cell with a boundary having two mechanical components. In panels (**a**–**c**), the inner layer grows and buckles to form two separate chambers, then both layers grow at constant curvature as in panel (**d**) until the original area and volume have doubled

for the most part the bilayer neck formed by the ring is flat and can be extended at no cost in deformation energy; in fact, the "hole" in the flat part of the membrane created by the ring possesses an edge tension that favors the contraction of the ring to form two separate chambers as in Fig. 2.7c. Of course, this is not a complete cell cycle, as the configuration in Fig. 2.7c still has the original volume and outer leaflet area as Fig. 2.7a; in fact, even the area of the inner leaflet has not doubled yet. However, if the time scale for the transfer of material from the inner to outer leaflets is not too long, the outer layer may now start to grow, allowing the enclosed volume to do likewise as in Fig. 2.7d.

Leaving aside the entropy-driven approach to cell division, we have described two "toy" models for the cell division cycle: (1) growth at constant curvature and (2) independent growth of bilayer leaflets. The time evolution of the length (L), surface area, and enclosed volume of the cell are different for each of these models: for growth at constant surface curvature, the cell elongates continuously, while in the independent leaflet model, the cell length is initially constant while the inner leaflet grows and buckles. Thus, there is a particular time dependence $L(t)$, $A(t)$, and $V(t)$ associated with the cell shape within each model for the division cycle. For living cells, this time dependence can be measured in the lab by photographing the growth of a single cell. Of course, this technique fails for microfossils, requiring the development of an alternate means of determining their division cycle. One such approach is based on the measurement of an ensemble of cells undergoing steady-state growth.

Suppose that we have an ensemble of n_{tot} cells whose shape we measure one by one. We assume that each cell started to grow at a random initial time, so the shapes of the cells in the sample are uncorrelated. Choosing a particular variable β (for example, length, area, volume...) we count that there are dn_β cells having a value of β between β and $\beta + d\beta$. Now, dn_β is a number, which necessarily depends on the total size of the sample n_{tot}. One can remove this dependence on the size of the experimental sample by constructing the probability density P_β (the probability per unit β) from the definition.

$$dn_{\backslash beta} = n_{tot}\, P_{\backslash beta}\, d\beta. \tag{2.10}$$

By integrating Eq. (2.10) over β, one finds that P_β is normalized to unity: $\int P_\beta\, d\beta = 1$. Note that P_β has units of β^{-1}, whereas dn_β is simply a number. The link between P_β and the time-dependence $\beta(t)$ is that under steady state conditions, P_β is given by

$$P_{\beta} = (\partial\beta / \partial t)^{-1} / T_2, \tag{2.11}$$

where T_2 is the doubling time of the cell cycle. For illustration, suppose the cell has the shape of a uniform cylinder that increases in length L from l to 2l (at fixed radius) whereupon it divides symmetrically at time T_2. If $L(t)$ grows linearly with time as $L(t) = (1 + t/T_2)$ l, then $P_l = 1/l$. In words, the physical meaning of Eq. (2.11) is that the more rapidly the quantity β changes, (i.e. larger $\partial\beta/\partial t$) the less time the cell spends in that range of β*/se* because $(\partial\beta/\partial t)^{-1}$ is small. This is familiar in the simple pendulum, which moves the fastest through its vertical position and slowest through its turning points, such that it is least likely to be found in the vertical position and most likely to be found at the turning points.

Next, consider the changes in shape of a diplococcus, which we represent as two intersecting spheres with the same radius R, like the outlines in Fig. 2.7. The cells in a single-species colony for either cyanobacteria or microfossils with the diplococcus shape are found to have uniformly similar radii, from which we conclude that the cells grow at constant width $2R$; their surfaces also appear to have curvature close to $1/R$. Thus, the length, area and volume of this family of shapes depend on only one geometrical quantity, which we choose to be the separation s between the centers of the intersecting spheres. Through the division cycle, the diplococcus grows from $s = 0$ (a single spherical cell) to $s = 2R$ (two spheres in contact), with the length L, area A, and volume V of the cell depending on s as

$$L = 2R(1+\beta) \tag{2.12a}$$

$$A = 4 \backslash \mathrm{pi}\, R^2 (1+\beta) \tag{2.12b}$$

$$V = (4 \backslash \mathrm{pi}\, R^3 / 3) \bullet [1+\beta(3-\beta^2)/2] \tag{2.12c}$$

where $\beta \equiv s/2R$. Once the time dependence of just one of L, A, or V is known, the time dependence of the remainder is determined and the probability densities P can be calculated from Eq. (2.11). It turns out that the volume appears to have the simplest functional dependence on time, with a linear increase in time or exponential increase in time being the most likely (Bennett et al. 2007):

Linear volume increase During the doubling time T_2, the rate of change of the volume is constant at $dV/dt = (4\pi R^3/3)/T_2$. The time dependence of the overall cell length can be found from this form, which then yields

$$p_{\beta} = 3(1-\beta^2)/2. \qquad (\mathrm{linear in} t) \tag{2.13}$$

Exponential volume increase In this situation, the rate at which the volume increases is proportional to the instantaneous value of the volume, or $dV/dt = V \ln 2/T_2$. From this,

$$p_{\beta} = [3(1-\beta^2)/\ln 2]/[2+\beta(3-\beta^2)]. \qquad (\mathrm{exponential in} t) \tag{2.14}$$

Although it might appear to be somehow more consistent to calculate P_V rather than P_β, the cell's length can be more accurately measured than its volume, so that P_β is the more useful quantity.

2.5 Evolution of the Division Cycle of Rod-Like Cells and Diplococci

The methodology described in Section 2.3 permits the determination of the time evolution of a quantity (such as the cell length) through the measurement of an ensemble of cells undergoing steady state growth. Being a statistical technique, a reasonably good size sample must be taken to ensure accuracy: this is achievable for colonies with 200 or more identifiable microfossils, although in the lab, samples with more than 600 cells are preferred. Analyses of, and comparisons between, two morphologies of modern and ancient cells have been performed thus far: rod-like cells and diplococci (also referred to as dyads in some contexts). For theoretical reasons, the diplococcus morphology is the more useful of the two, and is the focus of this section (which follows Bennett et al. 2007).

Three taxa of microfossils with the diplococcus morphology are displayed in Fig. 2.8, along with a rod-like taxon in the upper left-hand corner of the figure

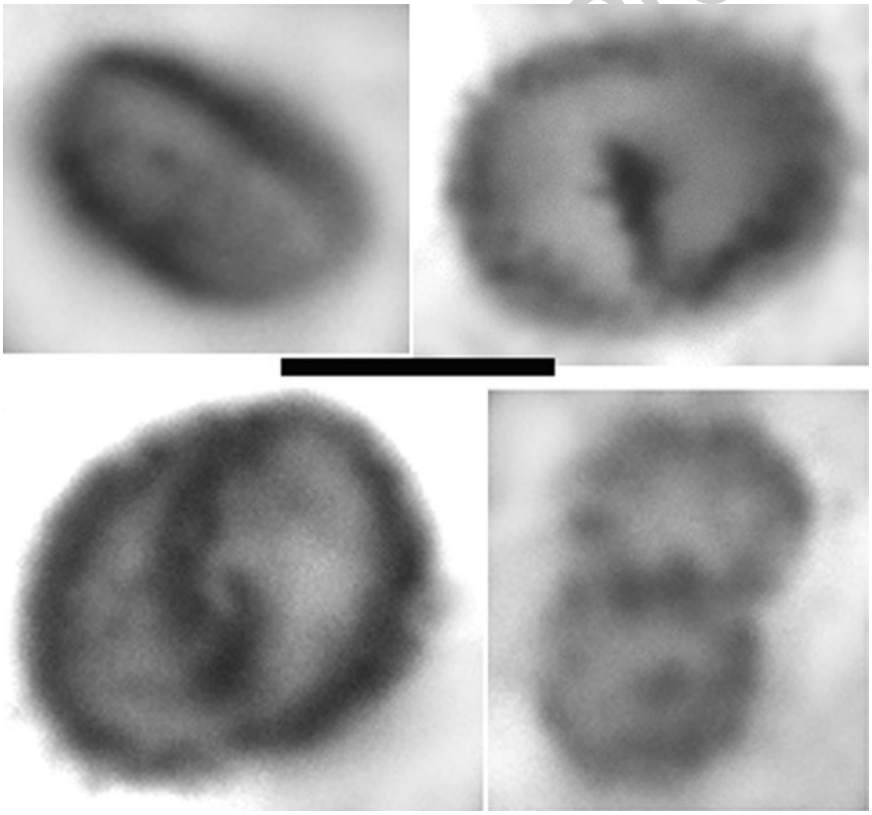

Fig.2.8 Examples of 2 Ga non-filamentous microfossils from the Belcher Island, Canada. Clockwise from the upper left: bacillus-like *E. moorei* and dyads *EB* (unclassified colony), *S. parvum*, and *E. belcherensis capsulata*. Scale bar, 5 µm (Bennett et al. 2007)

(microfossil specimens reported in Hofmann 1976). Modern diplococcal cyanobacteria have a very similar shapes, although the boundary is much crisper. In the strains described here, the smallest cells in a population are spherical, although there are some species where the smallest cells are slightly elongated, yet not so long as to be classified as bacillus-shaped. Colonies of ancient or modern diplococci all possess distributions in cell width that are very narrow: the standard deviation in cell width is less than 10% of the width itself. This suggests that the cells grow at fairly constant width, which is confirmed by scatter plots of cell width against cell length where only weak correlations are found to exist between the two variables. Thus, we are confident that Eq. (2.12) for L, A, and V of intersecting spheres with constant radius captures the shape of the cells to a good approximation.

The probability density P_β for the dimensionless separation $\beta = s/2R$ is shown in Fig. 2.9 for two species of the modern diplococcus *Synechocystis* from the Pasteur Culture Collection, PCC 6804 and PCC 6714 (Boal and Forde unpublished). The strains have spherical initial configurations such that there is complete overlap of the two mathematical surfaces describing the general diplococcal shape: *i.e.*, $s = 0$ and consequently $\beta = 0$. As a result, P_β is non-vanishing in the smallest measurable range of β. In fact, P_β is peaked around $\beta = 0$, above which it declines and eventully vanishes as

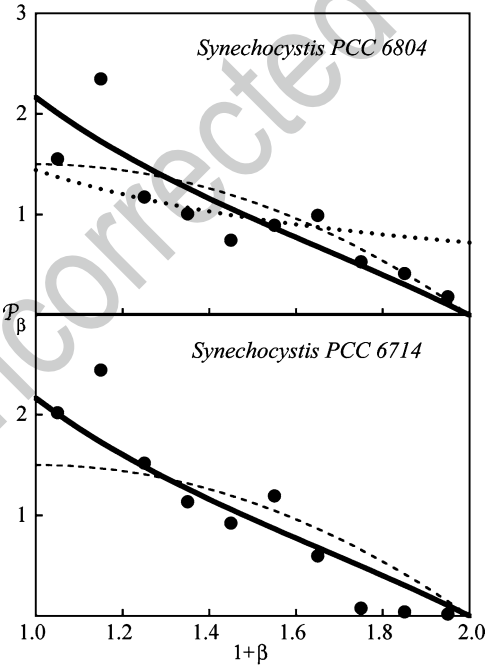

Fig.2.9 Probability density P_β as a function of β for *Synechocystis* diplococci PCC 6804 and PCC 6714. Shown for comparison are predictions from models based on exponential (*solid curve*) or linear (*dashed curve*) volume growth, as well as exponential growth of cell length or area (*dotted curve*, *top panel* only) (Boal and Forde unpublished)

$\beta \rightarrow 1$. This behavior of P_β has the physical interpretation that the cell grows most slowly at the start of its division cycle (large P_β) and most rapidly at its end (small P_β).

How do the measurements of P_β in Fig. 2.9 compare with models of cell growth? If the length or area of a diplococcus grows linearly with time from $\beta = 0$–1, then P_β is constant at unity for all β, clearly in disagreement with the measurements. Exponential growth based on cell length or area should obey $P_\beta = [\ln 2\ (1 + \beta)]^{-1}$, which decreases from 1.44 at $\beta = 0$–0.72 at $\beta = 1$. These values are well below the data in Fig. 2.9 at $\beta = 0$ and well above them at $\beta = 1$. In other words, neither of the length/area-based growth models with linear or exponential time dependence agrees with the observed behavior of P_β. The predicted P_β based upon volume growth with linear or exponential time dependence is also plotted in Fig. 2.9. The differences between the theoretical curves are obviously not large, which is expected because the exponential function e^x is approximately linear in x at small x. The intercept of P_β at $\beta = 0$ is predicted to be $3/(2\ \ln 2) = 2.16$ for exponential volume growth and 3/2 for linear volume growth. The higher (exponential) value of P_β ($\beta = 0$) is mildly preferred by experiment in both panels of the figure, but linear volume growth is not ruled out. This preference for exponential growth in volume is seen for many other cyanobacteria, including other diplococci as well as rod-like cells (Boal and Forde unpublished).

The lab specimens reported in Fig. 2.9 were prepared such that the symmetry axis of each cell was made to lie in the observational plane. In contrast, fossilized cells may have random orientations, so that either their shape must be reconstructed in three dimensions, or the analysis must take into account the orientation if the measured shapes are projections onto a plane. Here, we work with the unitless probability density P_Λ, where Λ is the projected cell length divided by the cell width (the width is unchanged by projection); Λ runs from 1 when $\beta = 0$–2, when $\beta = 1$. The correspondence between β and Λ is not unique, in that a range of configurations in β can contribute to a given Λ: for example, cells of any length may have $\Lambda = 1$ if their symmetry axis points towards the observer. Figure 2.10 displays P_Λ for three taxa of fossilized diplococci and the probability density is seen to rise rapidly to a maximum exceeding $P_\Lambda = 2.5$ at Λ near 1 before falling more gently as Λ approaches its upper limit of two for linked spheres. This behavior is very similar to that of P_β for modern diplococci in Fig. 2.9.

In terms of mathematical models for cell growth, it is not difficult to obtain P_Λ from P_β, and Fig. 2.10 contains the predictions of two models for the cell division cycle: exponential growth in volume (solid curve) and exponential growth in area (dashed curve). Exponential growth in area is a poor representation of the measured P_Λ, particularly at Λ near one, just as this same model failed to capture the behavior of P_β for modern diplococci. Linear growth in volume also underpredicts P_Λ at $\Lambda = 1$, where it approaches $3\pi/4 = 2.36$; P_Λ then exceeds the data as $\Lambda \rightarrow 2$ in this model. In contrast, exponential growth in volume corresponds most closely to both the quantitative and qualitative features of P_Λ seen in Fig. 2.10, and predicts $P_\Lambda(1) = 3.34$.

Let's now return to the principles behind the models for cell growth. Models where the growth of a cell is linear in time assume that change occurs at the same rate throughout the division cycle no matter what the contents of the cell. Examples

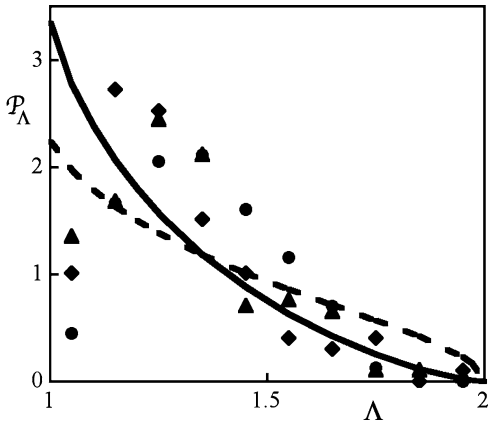

Fig. 2.10 Combined data for the probability density P_Λ of the dyads *S. parvum* (*diamonds*), *E. belcherensis capsulata* (*circles*), and an unclassified colony labeled *EB* (*triangles*) compared to the expectations of growth at constant curvature and exponential increase in volume (*solid curve*) or area (*dashed curve*). The largest values of P_Λ have about 30 cells per data bin for a statistical uncertainty of about 20% per individual datum (Bennett et al. 2007)

of linear models can be found in some eukaryotic cells, where cell mass grows linearly with time (Killander and Zetterberg 1965). Here, we observe that the only linear model not immediately ruled out by data is the linear rise in volume, for which agreement with data is marginal. Exponential growth may arise from several different mechanistic origins. Exponential growth in area corresponds to new surface being created at a rate proportional to the area available to absorb new material – a logical possibility but not supported by Fig. 2.10. Lastly, exponential growth in volume arises if new volume is created at a rate proportional to the cell's contents, which is the only scenario to comfortably describe the data. What we conclude from Figs. 2.9 and 2.10 is that exponential growth in volume has very likely been a guiding principle for the division cycle that was established at least two billion years ago for bacteria with the diplococcus morphology.

[AU4]

2.6 Summary

This article has examined the role that continuum and statistical mechanics plays in determining the size, shape and functionality of the simplest cell designs, focusing on cell morphologies such as diplococci and filaments that have at the most two important structural components. We described the bending resistance, edge tension and rupture resistance of lipid bilayers and showed the constraints that these elastic and mechanical properties place on the size of the simplest cells. For example, the rupture resistance of the bilayer generates a pressure-dependent cell radius beyond which a bilayer requires a cell wall for reinforcement. Similarly, the bending

resistance and edge tension of the bilayer set a minimal membrane area for the cell to spontaneously close into a spherical topology. Mechanical principles also may dominate the simplest or earliest forms of the cell division cycle. For example, the maximization of entropy can lead to a division cycle in which the membrane grows until it produces entropy-rich arms that can pinch off to form new cells if DNA replication and separation are appropriately choreographed. The minimization of deformation energy or of the consumption of materials also favors specific forms of the division cycle.

We investigated the mechanical features of cells more than two billion years old using a combination of statistical mechanics and comparisons between modern cyanobacteria and microfossils. In Section 2.2, we characterized the sinuous behavior of filamentous cells by means of a tangent correlation length ξ_t, demonstrated its power law dependence on filament diameter as D^n within a given genus, and provided an argument from continuum mechanics that this power law should have an exponent n in the range of 3–4. We also obtained soft bounds on the relationship between ξ_t and D for modern filamentous cyanobacteria according to the length-to-width ratio of individual cells within a filament, and then demonstrated that filamentous microfossils and pyritic replacement filaments satisfied these bounds. From this, we argued that the general mechanical features of filamentous cells were probably established relatively early in the development of life. Finally, in Section 2.4, we examined the division cycles of non-filamentous cells, focusing heavily on diplococci, in which we applied a technique that extracts the time dependence of a geometrical observable such as cell volume from an analysis of a colony of cells under steady-state growth conditions. It's found that that modern cyanobacteria and microfossils with rod-like or diplococcal shape are most consistent with exponential volume growth (although linear growth in volume cannot be ruled out). This argues that the volume of a cell increases with the volumetric contents of the cell, a division cycle that dates back at least two billion years.

References

Barghoorn ES, Schopf JW (1966) Microorganisms three billion years old from the Precambrian of South Africa. Science 152:758–763

Barghoorn ES, Tyler SA (1965) Microorganisms from the Gunflint chert. Science 147:563–577

Bennett S, Boal DH, Ruotsalainen H (2007) Growth modes of 2-Ga microfossils. Paleobiology 33:382–396

Boal DH (2002) Mechanics of the cell. Cambridge University Press, Cambridge

Boal DH, Rao M (1992) Topology changes in fluid membranes. Phys Rev A46:3037–3045

Bustamante C, Marko JF, Siggia ED, Smith S (1994) Entropic elasticity of Λ-phage DNA. Science 265:1599–1600

Cloud PE Jr (1965) Significance of the Gunflint (Precambrian) microflora. Science 148:27–35

Doi M, Edwards SF (1986) The theory of polymer dynamics. Oxford University Press, Oxford

Evans E, Rawicz W (1990) Entropy-driven tension and elasticity in condensed-fluid membranes. Phys Rev Lett 64:2094–2097

600 Fromhertz P (1983) Lipid-vesicle structure: size control by edge-active agents. Chem Phys Lett
601 94:259–266
602 Helfrich W (1973) Elastic properties of lipid bilayers: theory and possible experiments. Z Naturforsch
603 28c:693–703
604 Hofmann HJ (1976) Precambrian microflora, Belcher Islands, Canada: significance and systematics.
605 J Paleo 50:1040–1073
606 Luisi PL (2006) The emergence of life: from chemical origins to synthetic biology. Cambridge
607 University Press, Cambridge
608 Needham D, Hochmuth RM (1989) Electromechanical permeabilization of lipid vesicles. Biophys
609 J 55:1001–1009
610 Rasmussen B (2000) Filamentous microfossils in a 3.235-million-year-old volcanogenic massive
611 sulphide deposit. Nature 405:676–679
612 Schopf JW (1968) Microflora of the bitter springs formation, Late Precambrian, central Australia.
613 J Paleo 42:651–688
614 Schopf JW (1993) Microfossils of the early Archean Apex chert: new evidence of the antiquity of
615 life. Science 260:640–646
616 Schopf JW, Packer BM (1987) Early Archean (3.3-billion to 3.5 billion-year-old) microfossils
617 from Warrawoona Group, Australia. Science 237:70–73
618 Walsh MM, Lowe DR (1985) Filamentous microfossils from the 3, 500 Myr-old Onverwacht
619 Group, Barberton Mountain Land, South Africa. Nature 314:530–532
620 Zhu TF, Szostak JW (2009) Coupled growth and division of model protocell membranes.
621 J Am Chem Soc 131:5705–5713

Author Queries

Chapter No.: 2 0001195903

Queries	Details Required	Author's Response
AU1	Please provide the year for Boal and Ng.	
AU2	Please provide the year for Boal and Forde unpublished in the ref. list.	
AU3	Please include Boal and Jun unpublished in the ref. list.	
AU4	Please include Killander and Zetterberg 1965 in the ref. list.	